Pergamon

Tetrahedron 57 (2001) 8227–8235

TETRAHEDRON

Effect of the amino versus the acylamino substituent on the product isomer distribution in the methanolysis of 5-(substituted)-2-[(methylsulfonyl)oxy]isoindole-1,3-diones

John E. Kerrigan* and Lisa M. Vagnoni

Department of Pharmaceutical Chemistry, College of Pharmacy, Rutgers, The State University of New Jersey, 160 Frelinghuysen Road, Piscataway, NJ 08854, USA

Received 25 June 2001; accepted 7 July 2001

Abstract—The effect of the NH_2 versus the CH_3CONH and $PhCH_2CONH$ substituents at the 5-position in 5-(substituted)-2-[(methylsulfonyl)oxy]isoindole-1,3-diones, on the product isomer distribution resulting from methanolysis, was investigated both experimentally and at the RHF/3-21G*, RHF/6-31+G* and B3LYP/6-31+G* levels of theory. The influence of solvent on the transition structure was investigated using the Onsager SCRF model. The influence of these substituents on the transition state (TS) leading to tetrahedral intermediate was studied. The 5-amino (para to C-1) function makes the C-1 carbonyl carbon more electron-rich and less reactive toward nucleophilic attack. A predominance of the isomer formed from initial nucleophilic attack at C-3 is observed for the NH_2 substituent, whereas this selectivity is greatly reduced for the acylamino substituents. Examination of the LUMO from ab initio calculations performed on the starting materials at the RHF/6-31G* level give a good qualitative description of the regioselectivity observed from experiment. Calculated ΔE_a values of this initial reaction step give a qualitative description of the experimentally observed regioselectivity in agreement with the LUMO model and resonance argument.

1. Introduction

In an earlier investigation of 5-(substituted)amino-2-[(alkylsulfonyl)oxy]isoindole-1,3-diones, mechanism-based inhibitors of serine proteases, we observed the formation of two major products, with one product in predominance, in the buffer hydrolysis stability studies of these compounds.[1] The selectivity observed during buffer hydrolysis of these compounds is important in terms of the development of an inhibitor-enzyme binding model, and therefore warranted further investigation. Chapman and Freedman observed that *N*-[(trifluoromethylsulfonyl)oxy]phthalimide reacts with phenoxide preferentially through the imide carbonyl giving products resulting from a Lossen rearrangement.[2] It has been postulated by Fahmy and others from experimental observation that base-catalyzed nucleophilic attack on simple (R=H) isoindole-1,3-diones [i.e. (*N*-alkylsulfonyloxy)phthalimides] proceeds via the mechanism illustrated in Fig. 1.[3–5] The nucleophile (alcohol) attacks the carbonyl carbon of the dione to give a tetrahedral intermediate that leads to an intermediate that readily undergoes a Lossen rearrangement to give an isocyanate. This rearrangement is proposed to occur simultaneously in a concerted fashion.[6,7] Isotope effect studies of carboxylic acids which undergo the Schmidt reaction, a Lossen type rearrangement, indicate that the irreversible step leading to formation of the isocyanate is rate-determining.[8] The intermediate isocyanate undergoes further reaction with alcohol to give a carbamate-ester product. For those 2-[(alkylsulfonyl)oxy]-isoindole-1,3-diones bearing an R-substituent on the ring, two possible isomers can be formed from methanolysis. The hydrolysis products most likely result in the formation of anthranilic acids after a decarboxylation step. In studying this phenomenon, we decided to investigate the base-catalyzed methanolysis, as the product isomers were easier to separate and isolate.

In our initial approach, we decided to examine the lowest unoccupied molecular orbital (LUMO) of 5-amino-2-[(methylsulfonyl)oxy]-1*H*-isoindole-1,3(2*H*)-dione **1**. Intuitively, one may look at a simple resonance structure (Fig. 2). One can readily predict from the resonance structure of compound **1** that C-3 should be the more electrophilic carbonyl carbon, and therefore the isomer resulting from nucleophilic attack at C-3 should be the major product. The dipole moment of 5-amino-2-[(methylsulfonyl)oxy]-1*H*-isoindole-1,3(2*H*)-dione **1** (R=NH_2 in Fig. 1) is predicted to be larger than that of 2-[(methylsulfonyl)-oxy]-1*H*-isoindole-1,3(2*H*)-dione (R=H in Fig. 1) with no 5-substituent because of the greater charge separation in **1**. Comparison of the dipole moments calculated at the RHF/6-31G* level (compound **1** μ=7.9 D; vs μ=6.1 D for 2-[(methylsulfonyl)oxy]-1*H*-isoindole-1,3(2*H*)-dione) agree

Keywords: regioselectivity; transition structure; ab initio; density functional; methanolysis.

* Corresponding author. Tel.: +732-445-5763; fax: +732-445-6312; e-mail: jkerriga@cop.rutgers.edu

0040–4020/01/$ - see front matter
PII: S0040-4020(01)00827-4

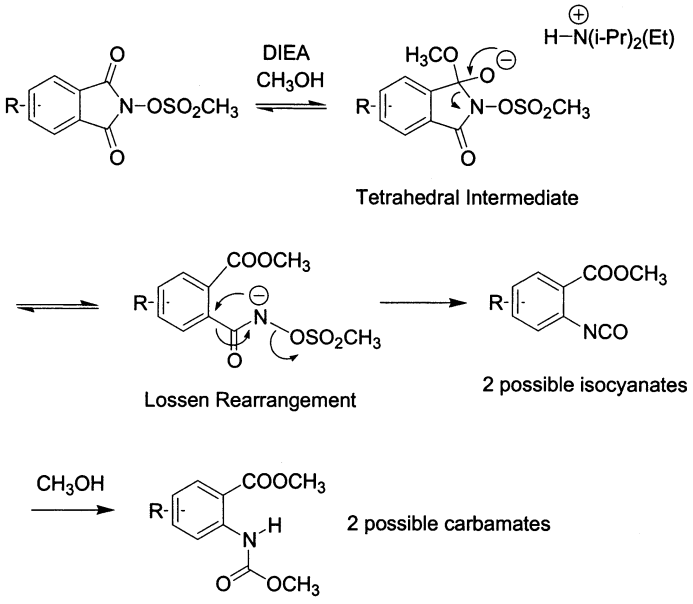

Figure 1. Methanolysis mechanism.

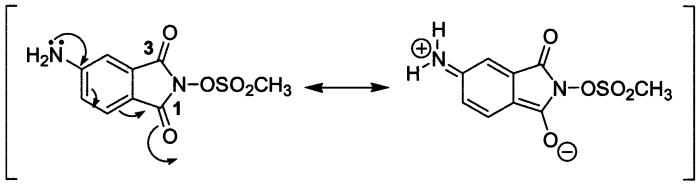

Figure 2. Compound **1** resonance structures.

with this prediction and lend support to the resonance argument. However, resonance arguments are not always correct in their assumptions. We opted to explore this problem further in comparing the LUMO (from RHF/6-31G* optimized geometry) of compound **1** to compound **2** (Figs. 3 and 4, respectively). Houk's application of Frontier Molecular Orbital (FMO) Theory toward the analysis of the LUMO of the electrophilic species in his investigation of the regioselectivity observed in nucleophilic additions to substituted benzoquinones and naphthoquinones clearly indicated a preference for nucleophilic attack at the vinylic carbon possessing the larger LUMO coefficient.[9] The LUMO density maps and coefficients clearly show a much larger orbital (blue) on C-3 compared to C-1 in the case of compound **1**, supporting the resonance argument. Although the magnitudes of the differences in the LUMO coefficients are small, they are of similar magnitude as those coefficient differences reported by Houk et al.[9] that

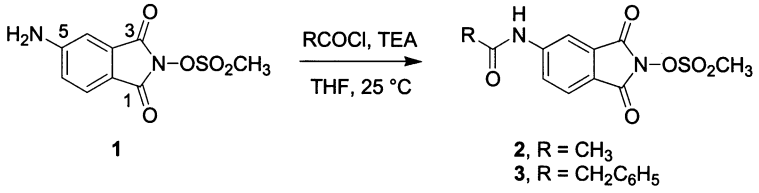

Scheme 1. Starting material preparation.

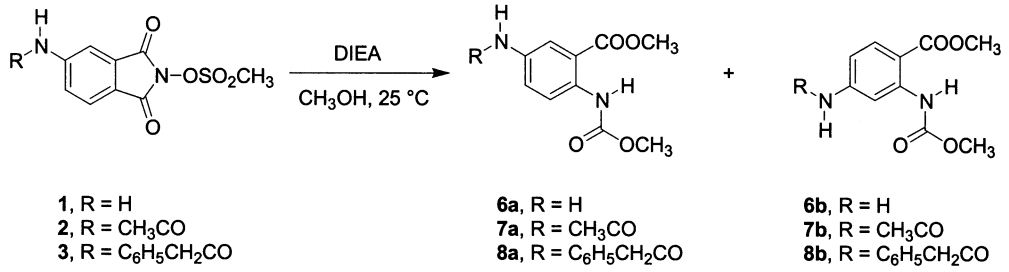

Scheme 2. Methanolysis study.

Table 1. Half-life data for reaction of compounds **1**–**3** with methanol and product ratios. Conditions: 25°C with DIEA (3 equiv.) added as the base

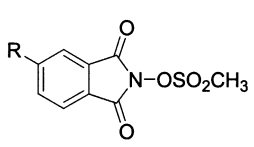

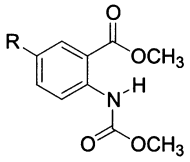

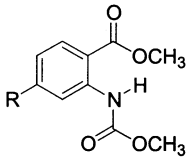

				Isomer **a**	Isomer **b**
Compound	R	$t_{1/2}$ (s)[a]	k_{obs} (s^{-1})[a]	Compound	Ratio (%**a**:%**b**)[b,c]
1	NH_2	99 (±1.7%)[d]	0.0070	**6a**:**6b**	87:13
2	CH_3CONH	17 (±3.5%)	0.0400	**7a**:**7b**	67:33
3	$C_6H_5CH_2CONH$	31 (±8.6%)	0.0210	**8a**:**8b**	58:42

[a] Values based on the average of duplicate runs.
[b] Ratio determined from HPLC data.
[c] Average relative standard deviation is ±2.0%.
[d] Number in parentheses is the relative percent standard deviation between the runs.

produce a high regioselectivity. This is also borne out in the LUMO density map and coefficients of compound **2**, which reveals a slightly larger orbital on C-3 relative to C-1.

2. Results and discussion

The starting materials for our study were prepared as shown in Scheme 1. Compound **1** was prepared exactly as described by Kerrigan and Shirley.[10] We used a tertiary amine base (diisopropylethylamine, DIEA) for the methanolysis study illustrated in Scheme 2. Kühle and Wegler used similar conditions in their report of the alcoholysis of simple nonsubstituted symmetric isoindole-1,3-diones.[5] We performed the assay using HPLC by monitoring the disappearance of the starting material peak with time as described in the Experimental Section. Under no circumstance for either column, did reaction products ever interfere with or overlap the starting material peak. Compound **1** is compared to the acylated analogs **2** and **3**. The half-life and product ratio data of the study are given in Table 1. In Fig. 5 is given a *psuedo*-first-order plot of the data for compound **3**. Compound **1** with R=NH_2 was the most stable to methanolysis under the conditions. Both acylated (R=R′CONH) analogs (**2** and **3**) were significantly more reactive toward methanolysis. Compound **2** was tenfold more reactive than compound **1**. The lone pair on nitrogen is an important factor in this reaction rate difference. The lone pair on nitrogen in compound **1** is free to donate its electron density to the isoindole-1,3-dione ring system. Whereas, in the acylated analogs (**2** and **3**) this lone pair is tied up in an amide bond, and is not freely donated to the isoindole-1,3-dione ring system. Therefore, compound **1** is more electron-rich and less electrophilic leaving it less reactive toward nucleophilic attack.

For the structure proof (Scheme 3), commercially available 2-amino-5-nitrobenzoic acid was esterified in refluxing

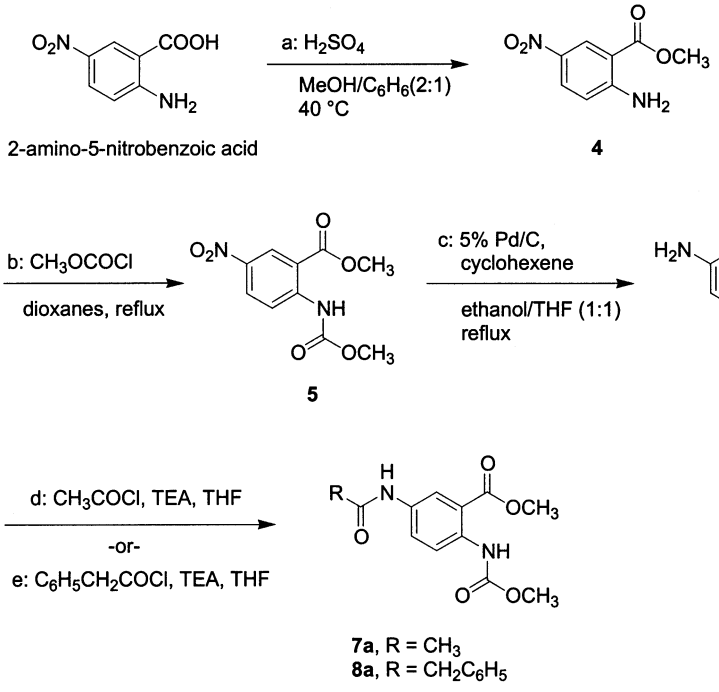

Scheme 3. Structure proof synthesis.

Table 2. Energies (kcal/mol) of reactant models and tetrahedral intermediate models

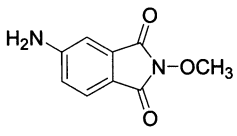

9

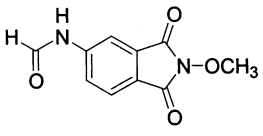

10

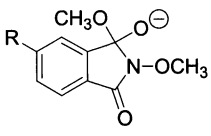

11a (R = NH_2)
12a (R = HCONH)

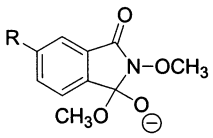

11b (R = NH_2)
12b (R = HCONH)

Compound	RHF/3-21G*	ΔE[a]	RHF/6-31G*[b]	ΔE[a]	RHF/6-31+G*[b]	ΔE[a]
CH_3O^-+**9**	−495,009.2	NA	−497,796.2	NA	−497,824.1	NA
CH_3O^-+**10**	−565,356.1	NA	−568,541.9	NA	−568,571.1	NA
11a	−495,068.8	−59.6	−497,834.4	−38.2	−497,856.2	−32.1
11b	−495,067.0	−57.8	−497,832.5	−36.3	−497,854.2	−30.1
12a	−565,421.8	−65.7	−568,586.4	−44.5	−568,609.3	−38.2
12b	−565,420.2	−64.1	−568,584.9	−43.0	−568,607.7	−36.6

[a] $\Delta E = E_{THI} - E_{SM}$.
[b] Single point on 3-21G* geometry.

methanol/benzene (2:1, v/v) using sulfuric acid in the preparation of **4** via the standard azeotropic removal of water with a Dean–Stark apparatus. Compound **4** was acylated with methyl chloroformate in refluxing dioxanes to form compound **5**. Reduction of the nitro group in compound **5** was achieved using a transfer-hydrogenation technique[11] in the preparation of compound **6a**. Reaction of compound **6a** with the appropriate acid chloride afforded compounds **7a** and **8a**.

The ratios of isomers **a** to **b** for each methanolysis reaction given in Table 2 were determined from HPLC data. The phenyl-hexyl column was used to separate the product isomers **a** and **b** for products **6** and **7**, while the C-18 column was sufficient to separate isomers **8a** and **8b**. Not surprisingly, the ratio of products produced from the methanolysis of compound **1** (**6a** and **6b**) shows a high selectivity in favor of isomer **a** (**6a**). This result supports our modeling study (Fig. 3), which revealed a much larger orbital on C-3 of the LUMO of compound **1**. The ratio of product isomers produced from methanolysis of compounds **2** and **3** shows a moderate selectivity in favor of isomer **a**. This result supports the 6-31G* LUMO picture in Fig. 4 showing a slightly larger orbital on C-3 as compared to C-1.

To support the LUMO study shown in Figs. 3 and 4, we

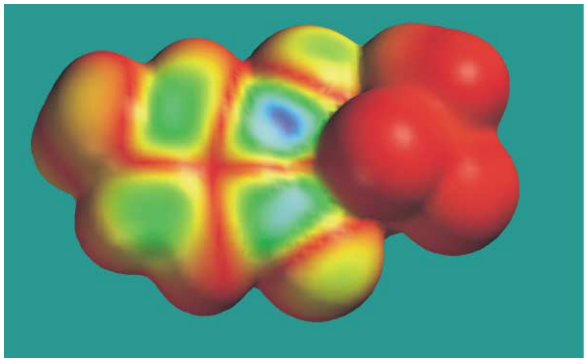

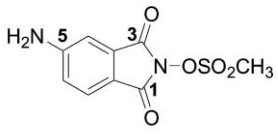

1 (μ = 7.9 D)

LUMO coefficients:

C-1 = 0.19 C-3 = 0.24

Figure 3. LUMO map, coefficients and dipole moment of **1** from RHF/6-31G* geometry optimization.

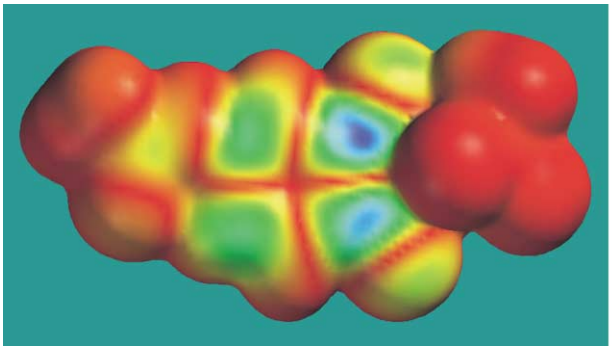

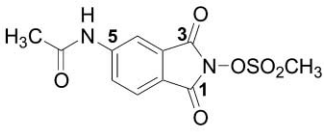

2 (μ = 8.6 D)

LUMO coefficients:

C-1 = 0.19 C-3 = 0.22

Figure 4. LUMO map, coefficients and dipole moment of **2** from RHF/6-31G* geometry optimization.

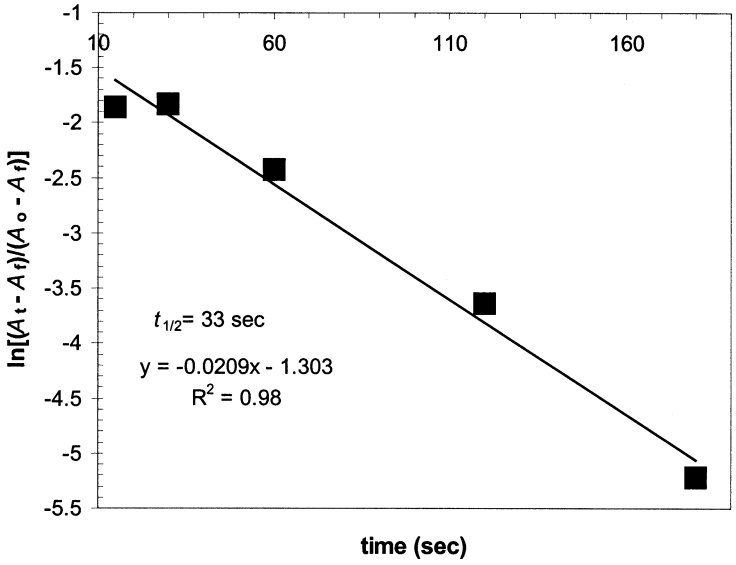

Figure 5. Compound **3** *pseudo*-first-order plot of methanolysis data.

initially investigated the transition structure leading to the formation of the intermediate isocyanate. However, our attempts to locate a transition structure for the Lossen rearrangement failed to converge for approach 'B'. In comparison, the initial addition of nucleophiles to the vinylic carbon of benzoquinone under base-catalyzed conditions is not rate-determining.[12] Nevertheless, Houk successfully applied FMO theory in his study of the LUMO of the benzoquinone to explain the regioselectivity observed in nucleophilic additions to substituted benzoquinones.[9] We decided to model the transition structure leading to formation of the tetrahedral intermediate. In development of this model, we assume that the regioselectivity observed will be determined predominantly by the interaction of the methoxide HOMO with the LUMO of the isoindole-1,3-dione in accordance with FMO theory.[13] Our goal here is to see whether or not the transition structure leading to the tetrahedral intermediate will reproduce the same qualitative trend as indicated by the LUMO model. To reduce computation time, we replaced the methylsulfonyl group with a methyl group (see Fig. 6) and opted to limit our geometry optimizations to the RHF/3-21G* level for these models. A study found that RHF/3-21G* geometries are suitable for transition structure analysis.[14] The formyl group was used as a replacement in the acyl analog. The transition structure optimization at the RHF/3-21G* level was performed from a 'guess' structure using the transition state geometry routine in TITAN (Wavefunction, Inc. and Schroedinger, Inc.).[15] The frequency calculations confirmed that these structures had a single imaginary vibration and qualify as potential transition states. From these data we estimated the activation energies (E_a) for approach to C-3 (TSA) compared to approach to C-1 (TSB) depicted in Fig. 5 for the amino substituted (TSA-A and TSB-A) and the formylamino substituted (TSA-F and TSB-F) compounds. The transition structures predicted by the RHF/3-21G* transition geometry calculation are 'early' transition structures on the reaction coordinate.

The data given in Table 2 outline the energies for the reactant models (**9** and **10**, each summed with methoxide anion) and the tetrahedral intermediate models: **11a**, **11b**, **12a**, and **12b**. The tetrahedral intermediates are all lower in energy relative to the reactants. Those tetrahedral intermediates resulting from approach 'A' (**11a** and **12a**) are lower in energy than those tetrahedral intermediates resulting from approach 'B' (**11b** and **12b**). Table 3 lists the activation energies ($E_a = E_{TS} - E_{(MeO^-}$ + **9** or **10**)) according to level of theory for each transition structure given in Fig. 6. Table 4 details the geometric parameters for the transition structures. From the geometric parameters listed in Table 4, we observe no difference between TSA-A and TSB-A, and only a slight difference between TSA-F and TSB-F. This is not surprising considering that the point of difference between these structures is distal to the site of reaction. Our geometric parameters for these transition states are in very good agreement with RHF/6-31G* gas-phase transition states for unassisted attack by the alcohol on formamide calculated by Warshel et al.[16] The unassisted attack model

Table 3. Energies (kcal/mol) of the transition structures and E_a

TS	RHF/3-21G*	E_a	RHF/6-31G*[a]	E_a	RHF/6-31+G*[a]	E_a
TSA-A	−494,903.6	105.6	−497,668.5	127.7	−497,690.8	133.3
TSB-A	−494,891.0	118.2	−497,654.9	141.3	−497,677.5	146.6
TSA-F	−565,247.4	108.7	−568,411.6	130.3	−568,434.9	136.2
TSB-F	−565,243.4	112.7	−568,407.5	134.4	−568,430.8	140.3

[a] Single point on 3-21G* geometry.

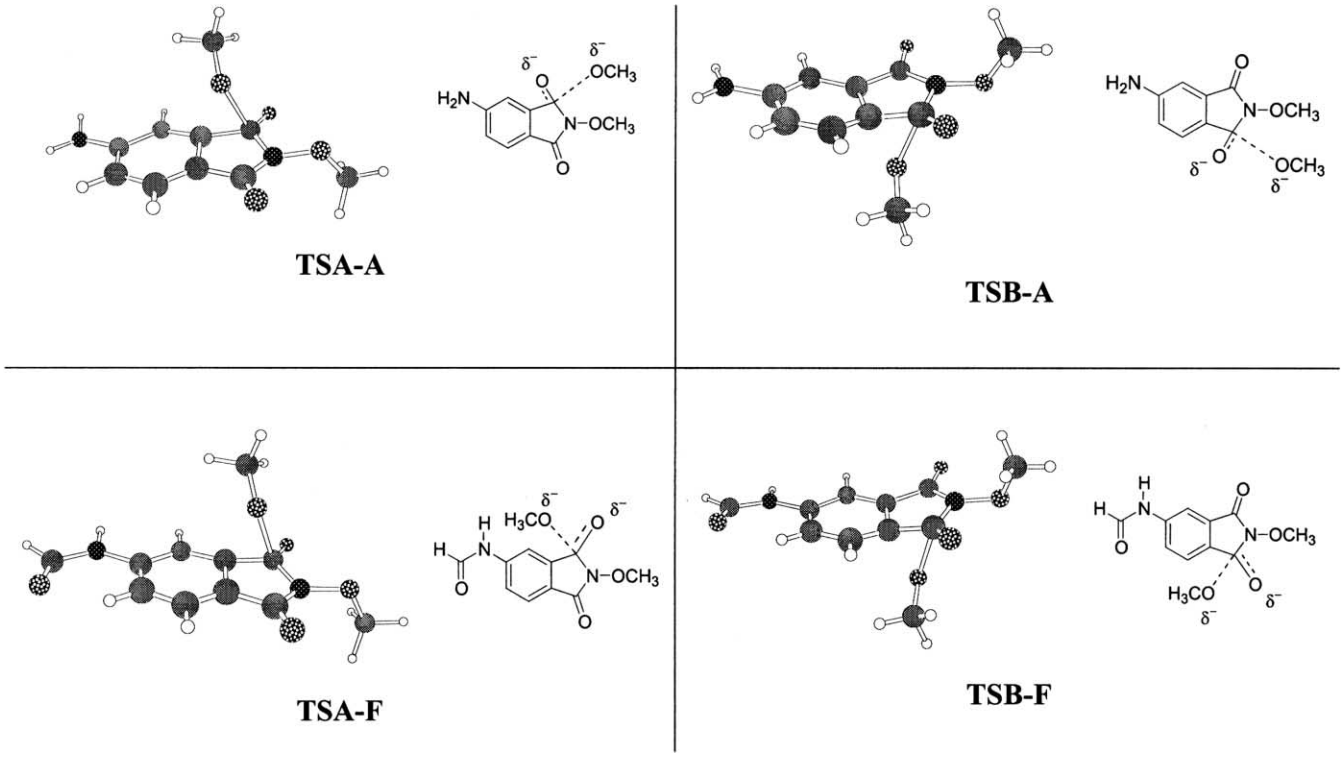

Figure 6. RHF/3-21G* geometry optimized transition structures: A=amino substituent; F=formylamino substituent.

Table 4. RHF/3-21G* geometry-optimized geometrical parameters for the transition structures (TS)

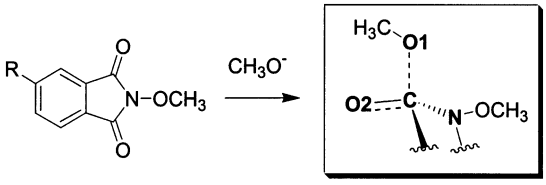

Parameter	**9** (R=NH_2)		**10** (R=HCONH)	
	TSA-A	TSB-A	TSA-F	TSB-F
C—N (Å)	1.405	1.405	1.404	1.406
C—O1 (Å)	1.992	1.992	1.995	2.004
C—O2 (Å)	1.222	1.222	1.221	1.220
O2—C—O1 (deg)	112.9	112.9	113.0	112.9
O2—C—N (deg)	124.4	124.4	124.6	124.4
O1—C—N (deg)	99.2	99.2	99.1	99.4

leads to higher energy transition states, which explains why our computed activation energy (E_a) values are large in magnitude relative to the experimentally determined activation energy for amide bond hydrolysis (E_a=+25.0 kcal/mol).[17] A 'concerted' complex transition state model including the base may be a better, more rigorous model; however, the computational cost of its implementation for our model was prohibitive.

Table 5 gives a breakdown of the energy differences associated with the two different approaches of the methoxide anion for both the tetrahedral intermediates and the transition structures broken down by level of theory. The difference in energy ($\Delta\Delta E$) between the tetrahedral intermediates resulting from both approaches A and B for both the amino and formyl substituents was close (−1.9 compared to −1.6 kcal/mol with approach 'A' being lower in energy). The difference in energy between the activation energies of the two different substituent models

Table 5. $\Delta\Delta E$ (kcal/mol) for tetrahedral intermediates and ΔE_a (kcal/mol) for transition structures

	$\Delta\Delta E$ (**11a**, **11b**)	$\Delta\Delta E$ (**12a**, **12b**)	ΔE_a (TSA-A–TSB-A)	ΔE_a (TSA-F–TSB-F)
RHF/3-21G*	−1.8	−1.6	−12.6	−4.0
RHF/6-31G*	−1.9	−1.5	−13.6	−4.1
RHF/6-31+G*	−2.0	−1.6	−13.3	−4.1
B3LYP/6-31+G*	−0.6	ND[a]	−7.4	−1.4
B3LYP/6-31+G*[b] (ε=32.6, MeOH)	−1.4	ND	−8.8	−2.8

[a] ND=not determined.
[b] SCRF data.

was more pronounced (−13.2 kcal/mol for R=NH_2 vs. −4.1 kcal/mol for R=HCONH). For both substituents, transition structure 'A' (TSA) was lower in energy. The larger energy difference between the two approaches (A and B) for R=NH_2 relative to the acyl analog R=HCONH is confirmed by the experimental results showing selectivity for product carbamate resulting from approach 'A'. The effect of the solvent (methanol) on the energy of the transition structure was investigated using the Onsager SCRF approach.[18–20] We used the Becke3LYP hybrid density functional theory (DFT) to account for electron correlation in the model.[21] The solvated models were all lower in energy relative to their gas-phase counterparts. The energy gaps (ΔE_a in Table 5) between TSA and TSB were smaller for the density functional calculations compared to the RHF calculations. Comparing the gas-phase B3LYP energy (E_{gp}) to the SCRF B3LYP energy (E_{solv}) reveals a larger energy gap due to greater stabilization of transition structure A (TSA) by solvation. The solvation stabilization ($E_{ss}=E_{gp}-E_{solv}$) for TSA-A was 2.9 kcal/mol compared to only 1.5 kcal/mol for TSB-A. A similar trend was observed in the formylamino models (E_{ss}=2.3 kcal/mol for TSA-F vs E_{ss}=1.0 kcal/mol for TSB-F). The tetrahedral intermediate **11a** realizes a greater benefit from solvation (E_{ss}=3.2 kcal/mol for **11a** vs E_{ss}=2.4 kcal/mol for **11b**) although to a slightly lesser extent. The magnitude of the ΔE_a values was too large for a reliable product ratio prediction using the Boltzmann equation. It may not be possible to quantitate the observed regioselectivity via this approach without a more in-depth examination (e.g. IRC calculation) of each individual mechanistic step leading up to and including the formation of the intermediate isocyanate (i.e. the rate-determining step).[7] Despite this limitation, modeling of the transition state leading to formation of the tetrahedral intermediate gives an excellent qualitative description of the regioselectivity observed experimentally. For all of the calculations reported here, the trend observed in the computed energy difference between TSA and TSB is supported by the experimental data.

3. Conclusion

Base-catalyzed methanolysis of 5-(substituted)amino-2-[(methylsulfonyl)oxy]isoindole-1,3-diones results in a mixture of isomeric isocyanates leading to a mixture of carbamates. Selectivity is governed by a more reactive electrophilic center at the C-3 carbonyl carbon of the isoindole-1,3-dione leading to a relatively more stable tetrahedral intermediate. This center is more reactive when the amine is not acylated; however, the electron-rich amine reduces the overall reactivity of the isoindole-1,3-dione toward base-catalyzed methanolysis. Acylation of the 5-amino function increases overall reactivity by making the overall molecule more electron-poor and reduces selectivity. We have demonstrated that simple gas-phase ab initio and SCRF DFT comparison of transition state structures leading to formation of the tetrahedral intermediate reproduce the same qualitative trend for the base-catalyzed methanolysis of 5-(substituted)amino-2-[(methylsulfonyl)-oxy]isoindole-1,3-diones as predicted by the LUMO model and resonance argument.

4. Experimental

4.1. General procedures

All reactions were performed under an inert atmosphere (N_2) in oven-dried glassware. All reagents were obtained either from Aldrich Chemical Co. or Acros Organics and used as supplied unless stated otherwise. Solvents were dried and distilled prior to use using standard procedures.[22] ^{1}H NMR spectra were recorded at 200 MHz using a Varian Gemini 2000 NMR spectrometer in the solvent indicated. Peak positions are recorded in ppm using either tetramethylsilane or the solvent peak as the internal reference. Thin layer chromatography was performed on aluminum plates coated with 254 nm fluorescent indicator with a layer thickness of 250 μm. Flash chromatography[23] was performed using silica gel from Scientific Adsorbents, Inc. (32–63 μm). Melting points were determined using a Mel-Temp II apparatus in open capillary tubes with a Fluke digital thermometer. All melting points are uncorrected. Elemental analyses were performed by Atlantic Microlab, Inc., Norcross, GA. Mass spectrometric analysis was performed by the Department of Chemistry, Washington University, St. Louis, MO. HPLC data were recorded on a Shimadzu Class VP HPLC using either a Phenomenex Luna 120 Å 5 μ phenyl-hexyl 4.6×150 mm analytical column or a YMS ODS-AQ (C-18) 120 Å 5 μ particle size 4.6×150 mm analytical column with UV detector set at 254 nm. The solvent mixtures used were acetonitrile with 25 mM NH_4OAc pH 5.4 buffer (30:70) as solvent A and acetonitrile (100%) as solvent B. The gradient was ramped from 100% solvent A to 100% solvent B in a linear fashion over a 10 min time period followed by 4 min with 100% solvent B. All HPLC runs were executed at a flow rate of 1.00 mL/min.

4.1.1. 5-Amino-2-[(methylsulfonyl)oxy]-1*H*-isoindole-1,3-(2*H*)-dione (1). This compound was prepared via the published procedure and crystallized from ethanol to give a yellow powder; mp 207.3–207.7°C dec, Lit.[10] 197–199°C dec.

4.1.2. 5-Acetylamino-2-[(methylsulfonyl)oxy]-1*H*-isoindole-1,3(2*H*)-dione (2). Triethylamine (0.6 mL, 4.7 mmol) was added to a THF (15 mL) solution of acetyl chloride (0.3 mL, 4.3 mmol) and **1** (1.0 g, 3.9 mmol) at room temperature. The mixture was allowed to stir at room temperature overnight. The solution was taken up in ethyl acetate (45 mL) and washed with 10% HCl (15 mL), saturated $NaHCO_3$ (2×8 mL), brine (15 mL), dried (Na_2SO_4) and concentrated. The crude precipitate obtained was recrystallized in THF/hexanes to give a light tan powder 930 mg, (80%): mp 178.0–180.6°C; ^{1}H NMR (DMSO) δ 10.67 (s, 1H), 8.27 (s, 1H), 7.22 (s, 2H), 3.63 (s, 3H), 2.14 (s, 3H); ^{13}C NMR (DMSO) δ 170.3, 162.7, 162.3, 146.4, 130.8, 126.3, 124.7, 122.6, 113.9, 25.0; MS *m/z* 298.0 (M^+); Anal. calcd. for $C_{11}H_{10}N_2O_6S$: C, 44.30; H, 3.38; N, 9.39. Found: C, 44.75; H, 3.60; N, 9.16.

4.1.3. 5-Phenacetylamino-2-[(methylsulfonyl)oxy]-1*H*-isoindole-1,3(2*H*)-dione (3). Triethylamine (0.9 mL, 6.7 mmol) was added to a THF (15 mL) solution of phenacetyl chloride (0.8 mL, 6.1 mmol) and **1** (1.42 g, 5.5 mmol) at

room temperature. The mixture was allowed to stir at room temperature for 18 h. This reaction was worked-up in the same manner as compound **2** above. The organic extracts yielded a crude precipitate, which was recrystallized in methanol to give a light yellow powder, 1.07 g (52%): mp 143.2–145.1°C (dec); ^{1}H NMR (DMSO) δ 10.89 (s, 1H), 8.27 (s, 1H), 7.99 (m, 2H), 7.25 (m, 5H), 3.63 (s, 2H), 3.58 (s, 3H); ^{13}C NMR (DMSO) δ 171.1, 162.6, 161.2, 146.2, 135.9, 130.8, 130.0, 129.1, 127.5, 126.3, 124.9, 122.8, 114.1, 44.1; MS *m/z* 373.7 (M^+); Anal. calcd. for $C_{17}H_{14}N_2O_6S$: C, 54.54; H, 3.77; N, 7.48. Found: C, 54.37; H, 3.81; N, 7.44.

4.1.4. 2-Amino-5-nitrobenzoic acid methyl ester (4). Sulfuric acid (1.4 mL, 26.2 mmol) was added to a methanol/benzene solution (20 mL:10 mL) of 2-amino-5-nitrobenzoic acid (2.0 g, 10.9 mmol). The mixture was allowed to reflux for 3 h. The reaction mixture was diluted in ethyl acetate (80 mL), washed with saturated $NaHCO_3$ (20 mL), brine (20 mL), dried ($MgSO_4$) and concentrated. The crude solid obtained was recrystallized from methanol to afford a bright yellow powder, 1.31 g (62%): mp 164.9–166.5°C. Lit.[24] 169–170°C.

4.1.5. 2-Methoxycarbonylamino-5-nitrobenzoic acid methyl ester (5). Methylchloroformate (1.6 mL, 20.4 mmol) was added to a solution of compound **4** (1.0 g, 5.1 mmol) in dioxanes (18 mL). This mixture was refluxed for 4.5 h. The mixture was added to water (20 mL) followed by extraction with ethyl acetate (2×60 mL). The combined ethyl acetate extracts were washed with brine (20 mL), dried (Na_2SO_4) and concentrated. The crude precipitate was purified by column chromatography (gradient elution: 16% ethyl acetate in hexanes to 75% ethyl acetate in hexanes) affording a light orange powder, 920 mg (71%): mp 169.0–171.5°C; ^{1}H NMR ($CDCl_3$) δ 10.91 (s, 1H), 8.95 (d, *J*=2.5 Hz, 1H), 8.70 (d, *J*=9.5 Hz, 1H), 8.42 (dd, *J*=9.7, 2.5 Hz, 1H), 4.01 (s, 3H), 3.87 (s, 3H); ^{13}C NMR ($CDCl_3$) δ 167.2, 165.0, 147.1, 141.3, 129.5, 127.2, 119.0, 114.2, 53.1, 53.0; MS *m/z* 254.1 (M^+); Anal. calcd. for $C_{10}H_{10}N_2O_6$: C, 47.25; H, 3.97; N, 11.02. Found: C, 47.40; H, 4.08; N, 11.04.

4.1.6. 5-Amino-2-methoxycarbonylaminobenzoic acid methyl ester (6a). To a vigorously stirred suspension of palladium (5% on carbon, 595 mg, 0.3 mmol) and compound **5** (710 mg, 2.8 mmol) in ethanol/THF (10 mL of a 1:1 v/v mixture) was added cyclohexene (1.7 mL, 16.8 mmol). The mixture was allowed to reflux for 1 h. The crude mixture was filtered over celite, washed with ethanol, and concentrated. The crude yellow powder obtained was used without further purification, 570 mg (91%): mp 102–103°C; ^{1}H NMR ($CDCl_3$) δ 10.80 (s, 1H), 8.20 (d, *J*=8.8 Hz, 1H), 7.34 (d, *J*=2.9 Hz, 1H), 6.94 (dd, *J*=8.8, 2.9 Hz, 1H), 3.91 (s, 3H), 3.77 (s, 3H), 3.60 (bs, 2H); ^{13}C NMR ($CDCl_3$) δ 168.4, 154.4, 140.8, 133.7, 122.0, 120.5, 116.3, 115.8, 52.3, 52.2; MS *m/z* 224.1 (M^+); Anal. calcd. for $C_{10}H_{12}N_2O_4$: C, 53.57; H, 5.39; N, 12.49. Found: C, 53.75; H, 5.34; N, 12.23.

4.1.7. 5-Acetylamino-2-methoxycarbonylaminobenzoic acid methyl ester (7a). Triethylamine (0.1 mL, 1.1 mmol) was added to a THF (3 mL) solution of compound **6a** (200 mg, 0.9 mmol) and acetyl chloride (0.1 mL, 1.0 mmol) at room temperature. The mixture was allowed to stir at room temperature for 0.5 h. The mixture was diluted in ethyl acetate (10 mL), washed with 10% HCl (3 mL), saturated $NaHCO_3$ (2×3 mL), brine (3 mL), dried (Na_2SO_4) and concentrated giving a crude precipitate. The crude solid was recrystallized in ethyl acetate/hexanes to yield a tan solid 210 mg (89%): mp 230.0–230.7°C; ^{1}H NMR (DMSO) δ 10.08 (d, 1H), 10.03 (d, 1H), 8.23 (d, *J*=2.6 Hz, 1H), 8.04 (d, *J*=9.2 Hz, 1H), 7.77 (dd, *J*=9.2, 2.6 Hz 1H), 3.85 (s, 3H), 3.68 (s, 3H), 2.03 (s, 3H); ^{13}C NMR (DMSO) δ 169.1, 168.3, 154.3, 136.0, 134.8, 125.6, 121.3, 120.8, 117.4, 53.2, 52.9, 24.6; MS *m/z* 266.2 (M^+); Anal. calcd. for $C_{12}H_{14}N_2O_5$: C, 54.13; H, 5.30; N, 10.52. Found: C, 53.75; H, 5.39; N, 10.47.

4.1.8. 5-Phenacetylamino-2-methoxycarbonylaminobenzoic acid methyl ester (8a). Triethylamine (0.03 mL, 0.3 mmol) was added to a THF (3 mL) solution of compound **6a** (50 mg, 0.2 mmol) and phenacetyl chloride (0.03 mL, 0.3 mmol) at room temperature. The mixture was allowed to stir for 0.5 h. The mixture was worked-up in the exact same manner as for compound **7a**. The crude precipitate obtained was recrystallized in ethyl acetate/hexanes to give the compound as a cream-colored powder 50 mg (78%): mp 187.0–188.0°C; ^{1}H NMR ($CDCl_3$) δ 10.40 (s, 1H), 8.35 (d, *J*=9.2 Hz, 1H), 8.22 (d, *J*=2.6 Hz, 1H), 7.22–7.50 (m, 7H), 3.89 (s, 3H), 3.78 (s, 3H), 3.75 (s, 2H); ^{13}C NMR ($CDCl_3$) δ 169.3, 168.1, 154.2, 138.5, 134.3, 131.6, 129.6, 129.4, 127.9, 126.6, 122.4, 119.5, 114.9, 52.5, 52.4, 44.7; MS *m/z* 342.2 (M^+); Anal. calcd. for $C_{18}H_{18}N_2O_5$: C, 63.15; H, 5.30; N, 8.18. Found: C, 62.88; H, 5.47; N, 8.19.

4.2. General procedure for the methanolysis assay

For all methanolysis assays, 5 mg of **1**, **2**, or **3** was taken up in methanol (5 mL) at 25°C. All of the compounds were tested for stability to the mildly acidic conditions of the HPLC buffer system. All standards were found to be stable to the HPLC conditions. The phenyl-hexyl column was used for the analysis of the methanolysis of compounds **1** and **2**. The C-18 column was used for the analysis of the methanolysis of compound **3**. Base-catalyzed methanolysis was initiated by the addition of diisopropyl ethylamine (3 equiv.). The half-life of compound methanolysis was determined by monitoring the decrease in peak area of the starting material. Plots of $\ln[(A_t-A_f)/(A_o-A_f)]$ vs time (s) [where A_t and A_f are the peak areas of the starting material at times t and the final reading and A_o is the initial peak area (i.e. before addition of base)] were linear and used to determine the methanolysis rate. Half-life values were calculated using the first-order relationship $t_{1/2}=0.693/k$, where k (s^{-1}) was obtained from the slope of the line. The methanolysis products were isolated and purified by flash chromatography (silica gel) using a gradient elution method. (Gradients are listed by starting material compound number. **1**: 20% ethyl acetate in hexanes to 80% ethyl acetate with 10% methanol in hexanes; **2**: 25% ethyl acetate in hexanes to 86% ethyl acetate with 5% methanol in hexanes; **3**: 16% ethyl acetate in hexanes to 75% ethyl acetate in hexanes.) Isomer assignments were determined with the assistance of the synthetic structure proof.

4.2.1. 4-Amino-2-methoxycarbonylaminobenzoic acid (6b). Melting point 125.6–129.3°C; ^{1}H NMR ($CDCl_3$) δ 10.75 (s, 1H), 7.80 (d, J=8.8 Hz, 1H), 7.74 (d, J=2.2 Hz, 1H), 6.28 (dd, J=8.8, 2.2 Hz, 1H), 4.17 (s, 2H), 3.86 (s, 3H), 3.78 (s, 3H); ^{13}C NMR ($CDCl_3$) δ 168.6, 154.3, 152.4, 143.8, 133.0, 108.1, 104.7, 103.0, 52.3, 51.8; MS m/z 224.0 (M^+); Anal. calcd. for $C_{10}H_{12}N_2O_4$: C, 53.57; H, 5.39; N, 12.49. Found: C, 53.74; H, 5.37; N, 12.28.

4.2.2. 4-Acetylamino-2-methoxycarbonylaminobenzoic acid (7b). Melting point 191.5–191.7°C; ^{1}H NMR ($CDCl_3$) δ 10.60 (s, 1H), 8.19 (d, J=1.8 Hz, 1H), 8.01 (d, J=8.8 Hz, 1H), 7.74 (d, J=8.1 Hz, 1H), 7.61 (s, 1H), 3.88 (s, 3H), 3.70 (s, 3H), 2.21 (s, 3H); ^{13}C NMR ($CDCl_3$) δ 185.7, 168.2, 154.3, 143.6, 142.6, 132.7, 112.7, 110.2, 108.0, 52.4, 52.2, 24.9; MS m/z 266.1 (M^+); Anal. calcd. for $C_{12}H_{14}N_2O_5$: C, 54.13; H, 5.30; N, 10.52. Found: C, 54.04; H, 5.31; N, 10.27.

4.2.3. 4-Phenacetylamino-2-methoxycarbonylaminobenzoic acid methyl ester (8b). Melting point 209.9–210.2°C; ^{1}H NMR ($CDCl_3$) δ 10.60 (s, 1H), 8.10 (d, J=2.3 Hz, 1H), 7.95 (d, J=9.2 Hz, 1H), 7.69 (dd, J=9.2, 2.1 Hz, 1H), 7.28–7.47 (m, 6H), 3.89 (s, 3H), 3.77 (s, 3H), 3.75 (s, 2H); ^{13}C NMR ($CDCl_3$) δ 169.6, 168.2, 154.2, 143.4, 142.5, 134.0, 132.5, 129.5, 129.3, 127.9, 112.9, 110.4, 108.3, 52.4, 45.1; MS m/z 342.0 (M^+); Anal. calcd. for $C_{18}H_{18}N_2O_5\cdot(H_2O)_{0.5}$: C, 61.83; H, 5.45; N, 7.97. Found: C, 61.74; H, 5.27; N, 7.95.

4.3. Molecular modeling

All computations were carried out on a Dell Precision 620 Workstation using TITAN (Wavefunction, Inc. and Schroedinger, Inc.). All structure models were initially geometry optimized using the Merck Molecular Force Field (MMFF94).[25] The structure models for compounds **1** and **2** depicted in Figs. 3 and 4 were geometry optimized at the RHF/6-31G* level of theory.[26] All single point and SCRF calculations employing the RHF/6-31G*, RHF/6-31+G* and B3LYP/6-31+G* methods were performed in Gaussian 98 using 'tight' convergence criteria.[27]

Acknowledgements

The authors wish to thank the New Jersey Thoracic Society of the American Lung Association and the Charles and Johanna Busch Foundation for their generous support. In addition, the authors wish to thank the referees of this journal for their intuitive comments and suggestions.

References

1. Vagnoni, L. M.; Gronostaj, M.; Kerrigan, J. E. *Bioorg. Med. Chem.* **2001**, *9*, 637–645.
2. Chapman, T. M.; Freedman, E. A. *J. Org. Chem.* **1973**, *38*, 3908–3911.
3. Harger, M. J. P. *J. Chem. Soc., Perkin Trans. I* **1983**, 2699–2702.
4. Fahmy, A. F. M.; Aly, N. F.; Nada, A.; Aly, N. Y. *Bull. Chem. Soc. Jpn.* **1977**, *50*, 2678–2681.
5. Kühle, E.; Wegler, R. *Justus Leibigs Ann. Chem.* **1958**, *616*, 183–206.
6. Berndt, D. C.; Shechter, H. *J. Org. Chem.* **1964**, *29*, 916–918.
7. Lowry, T. H.; Richardson, K. S. *Mechanism and Theory in Organic Chemistry*; 3rd; Harper & Row: New York, 1987.
8. Rabinowitz, J. L.; Chase, G. D.; Kaliner, L. F. *Anal. Biochem.* **1967**, *19*, 578–583.
9. Rozeboom, M. D.; Tegmo-Larsson, I. M.; Houk, K. N. *J. Org. Chem.* **1981**, *46*, 2338–2345.
10. Kerrigan, J. E.; Shirley, J. J. *Bioorg. Med. Chem. Lett.* **1996**, *6*, 451–456.
11. Entwistle, I. D.; Johnstone, R. A. W.; Povall, T. J. *J. Chem. Soc., Perkin Trans. I* **1975**, 1300–1301.
12. Ogata, Y.; Sawaki, Y.; Isono, M. *Tetrahedron* **1969**, *25*, 2715–2721.
13. Fleming, I. *Frontier Orbitals and Organic Chemical Reactions*; Wiley: New York, 1976.
14. Rosenberg, R. E.; Mohrig, J. R. *J. Am. Chem. Soc.* **1997**, *119*, 487–492.
15. Schlegel, H. *J. Comput. Chem.* **1982**, *3*, 214–218.
16. Strajbl, M.; Florian, J.; Warshel, A. *J. Am. Chem. Soc.* **2000**, *122*, 5354–5366.
17. Radzicka, A.; Wolfenden, R. *J. Am. Chem. Soc.* **1996**, *118*, 6105–6109.
18. Wong, M. W.; Frisch, M. J.; Wiberg, K. B. *J. Am. Chem. Soc.* **1991**, *113*, 4776–4782.
19. Wong, M. W.; Wiberg, K. B.; Frisch, M. J. *J. Am. Chem. Soc.* **1992**, *114*, 1645–1652.
20. Wiberg, K. B.; Wong, M. W. *J. Am. Chem. Soc.* **1993**, *115*, 1078–1084.
21. Kohn, W.; Becke, A. D.; Parr, R. G. *J. Phys. Chem.* **1996**, *100*, 12974–12980.
22. Perrin, D. D.; Armarego, W. L. F. *Purification of Laboratory Chemicals*; 3rd; Pergamon Press: New York, 1988.
23. Still, W. C.; Kahn, M.; Mitra, A. *J. Org. Chem.* **1978**, *43*, 2923–2925.
24. Makosza, M.; Bialecki, M. *J. Org. Chem.* **1998**, *63*, 4878–4888.
25. Halgren, T. *J. Comput. Chem.* **1996**, *17*, 490–519.
26. Hehre, W.; Radom, L.; Schleyer, P.; Pople, J. *Ab Initio Molecular Orbital Theory*; Wiley: New York, 1986.
27. Frisch, M.; Trucks, G.; Schlegel, H.; Scuseria, G.; Robb, M.; Cheeseman, J.; Zakrzewski, V.; Montgomery, J.; Stratmann, R.; Burant, J.; Dapprich, S.; Millam, J.; Daniels, A.; Kudin, K.; Strain, M.; Farkas, O.; Tomasi, J.; Barone, V.; Cossi, M.; Cammi, R.; Mennucci, B.; Pomelli, C.; Adamo, C.; Clifford, S.; Ochterski, J.; Petersson, G.; Ayala, P.; Cui, Q.; Morokuma, K.; Malick, D.; Rabuck, A.; Raghavachari, K.; Foresman, J.; Cioslowski, J.; Ortiz, J.; Baboul, A.; Stefanov, B.; Liu, G.; Liashenko, A.; Piskorz, P.; Komaromi, I.; Gomperts, R.; Martin, R.; Fox, D.; Keith, T.; Al-Laham, M.; Peng, C.; Nanayakkara, A.; Challacombe, M.; Gill, P.; Johnson, B.; Chen, W.; Wong, M.; Andres, J.; Gonzalez, C.; Head-Gordon, M.; Replogle, E.; Pople, J.; *Gaussian 98*, Revision A.9, Gaussian, Inc., Pittsburgh, PA, 1998.